



## Nitrate removal by nanofiltration and reverse osmosis: comparison and modeling

Hajar Zeggar\*, Fatima Zahra Addar, Soufian El-Ghizizel, Sara Kitanou, Mustapha Tahaikt, Mohamed Taky, Azzedine Elmidaoui

Laboratory of Advanced Materials and Process Engineering, Faculty of Sciences, Ibn Tofail University, P.O. Box: 1246, Kenitra, Morocco, emails: zeggar.hajar@uit.ac.ma (H. Zeggar), fatima.zahra@uit.ac.ma (F.Z. Addar), soufian.el-ghizizel@uit.ac.ma (S. El-Ghizizel), sarra.kitanou@gmail.com (S. Kitanou), mustapha.tahaikt@uit.ac.ma (M. Tahaikt), mohamed.taky@uit.ac.ma (M. Taky), elmidaoui@uit.ac.ma (A. Elmidaoui)

Received 2 October 2023; Accepted 7 December 2023

### ABSTRACT

The aim of this research is to compare the influence of initial ion concentration on nitrate transfer in nanofiltration (NF) and reverse osmosis (RO) membranes. To accomplish this study, three mathematical models were employed: Kedem–Katchalsky (KK), Spiegler–Kedem (SK), and Nernst–Planck model coupled with film theory (NP-FT). While the KK and SK models do not consider the concentration polarization layer (CP) or electrostatic interaction, they can determine the convective concentration ( $C_{conv}$ ), diffusive flux ( $J_{diff}$ ), reflection coefficient ( $\sigma$ ), and permeability ( $P_s$ ) of nitrate ions. The NP-FT model considers the impact of the CP layer and enables the assessment of the thickness ( $\delta$ ) of the CP layer,  $P_s$ , and  $\sigma$ . The research was conducted on actual groundwater that was doped with  $\text{NaNO}_3$  at various initial nitrate concentrations (IC) (50, 100, 200, 300, and 400 mg/L) using the NE90 membrane for NF and RE-BN for RO. The obtained results indicate that the rejection of nitrate ions depends on the pressure and initial concentration, with a more significant dependence observed in the case of the NE90 membrane. The KK and SK models' parameters ( $C_{conv}$ ,  $J_{diff}$ ,  $P_s$ , and  $\sigma$ ) depend on the IC, but this dependence is more pronounced for NF than RO. Both types of ion transfer, convection and diffusion, are present in both membranes with a predominance of diffusion, and their contribution depends on IC. The thickness  $\delta$  determined by the NP-FT model for both membranes was negligible for RO, and about  $10^{-8}$  m for NF.

**Keywords:** Nitrate removal; Membrane; Modeling; Transfer mechanisms; Kedem–Katchalsky model; Spiegler–Kedem model; Nernst Plank equation; Film theory

### 1. Introduction

Nitrate pollution in surface water and groundwater is a global concern. According to the literature, 292 regions in the world are affected by nitrate pollution, and 60 of these regions are under a critical situation [1,2], including Brazil [3], Belgium [4], Congo [5], Morocco [6–8], Palestine [9], Pakistan [10], India [11] and China [12]. The population explosion, excessive pollution and industrialization are the main reasons. The presence of nitrates in water is generally

anthropogenic, following the use of high doses of chemical fertilizers, industrial pollution and livestock manure, and leachate from landfill sites, through which nitrate-rich material present on earth seeps into the soil to reach the water table [13–16].

In recent years, global water contamination by nitrate has emerged as a significant concern for both human life and the environment. The growing concern about the presence of this contaminant in groundwater is evident from

\* Corresponding author.

Presented at the 3rd International Congress on Separative Techniques Facing the Challenges of Sustainable Development (Francofilt 2023), 10–12 May, 2023, Fez, Morocco

the escalating number of articles dedicated to this topic. The number of manuscripts addressing this issue increased from 20 in 1990 to 280 in 2021, indicating a significant rise in interest and attention to this subject [1]. The elevated concentration of nitrates has severe consequences on marine ecosystems, leading to toxic algal blooms, eutrophication, and hypoxia [17]. On the other hand, the presence of high nitrate levels in drinking water can pose health risks to humans, such as methemoglobinemia in children, diabetes, spontaneous abortion in pregnant women, thyroid disease, and stomach cancer in adults [18]. In response to these concerns, the World Health Organization (WHO) has set a maximum allowable nitrate content in drinking water at 50 mg/L [19]. The same value is adopted in Morocco [20].

Various technologies have been developed to solve the problem of nitrate pollution from groundwater, wastewater and surface water including physical, chemical and biological methods. Among them, electrodialysis requires consideration of time, temperature, flow and voltage to be optimized, loss of efficiency due to fouling and scaling. Among its advantages: this technology leads to high reduction efficiency and environmentally friendly [21–24]. Ion exchange is a simple, efficient and selective technology. However, this technology represents less affinity for nitrates compared to sulfates [25–27]. Denitrification is an environmentally friendly technology, and it has the disadvantages of a high installation cost, maintenance issues and bacteria sludge [28,29]. Membrane separation is considered by many environmental researchers to be an effective method of nitrate removal [30–33]. Nanofiltration (NF) and reverse osmosis (RO) are emerging as highly effective treatment methods for removing nitrates from water [34–37]. Based on the membrane material, ceramic membranes, due to their porosity accompanied by narrow pore size, are beneficial for high flux, appreciable separation properties, as well as durability having the provision of backwashing, efficiency and mechanical stability, simplicity in operation devoid of additives [38]. It was reported that the complexity of the ionic composition of solute has a negative effect on the rejection of nitrate. An increase in initial nitrate concentration in feed solution is found to cause a decline in rejection of nitrate due to polarization phenomena. As well low sulfate concentration and low mineralization lead to best nitrate rejection. It has been demonstrated also that the best nitrate rejection is obtained when adding a divalent cation instead of a monovalent cation, due to improved hydration radius causing repulsion [2].

The solution diffusion model is the most widely used theory to explain the mass transfer mechanism and membrane selectivity of RO. However, for NF, the mechanism appears to be more complex and may vary not only with pore size but also with other membrane characteristics. The forces that influence the ions passing through NF membranes are columbic, dielectric, and hydration forces. The significance of each of these forces will depend on the molecules, the membrane, and the operating conditions such as pressure and concentration of the solution. Numerous models have been developed to depict and forecast the flow and rejection of diverse substances in various operational scenarios for this both membranes [39]. The commonly utilized models include the Kedem–Katchalsky (KK) model [40], the

Spiegler–Kedem (SK) model, and models derived from the Nernst–Planck equation [41].

The KK model is founded on the principle that solvent movement is a result of a pressure gradient existing across the membrane, while solute transport occurs due to either a concentration gradient ( $J_{diff}$ ) or convective ( $C_{conv}$ ) coupling volume flow [42,43]. Solute transport in NF and RO membranes is governed by the charged active layer of the membrane and is attributed to a combination of steric effects, as well as differences in solute diffusivity and solubility [44]. In NF membranes, besides these mechanisms aforementioned, the Donnan effect and dielectric influence the transport of solutes [45]. This model neglects the electrostatic interaction between the membrane and the solutes and the phenomenon of concentration polarization. On the other hand, the SK model is based on irreversible thermodynamics. It describes the transport of solutes across a membrane using non-equilibrium thermodynamic principles, treating the membrane as a black box. This approach allows characterizing the membranes solely in terms of the reflection coefficient ( $\sigma$ ) and solute permeability ( $P_s$ ). The phenomenological parameters in this model might exhibit dependency on solute concentration if the forces are strong enough [46].

Many authors used the combined model (KK, SK) to study electrolyte rejection in charged membranes [39,47–52]. However, the modeling of nitrate rejection by NF and RO membranes using this model is almost nil. In our previous study, we used the SK and KK to study nitrate and other anions rejections involved contained in nitrated brackish water by using a polyamide NE90 and BW30 membranes. The results showed that  $\sigma$  and  $P_s$  depend on the nature of anion, and the transport mechanism in NE90 and BW30 is convective and diffusional, with the preponderance of diffusion for BW30 [53].

The other model that can describe the transfer of nitrate rejection in NF and RO membranes proposed by Chaabane et al. [54] is based on the extended Nernst–Planck equation coupled with film theory (NP-FT). This model takes into consideration the previously neglected polarization layer by SK model. Concentration polarization is assumed to occur within a boundary film adjacent to the membrane/feed solution interface. The concentration of the solute in this layer increases in comparison with its feed concentration. A concentration gradient is established on this layer, from the membrane surface, where the concentration is highest, to the bulk of the feed solution, which has the lowest concentration. The boundary layer thickness  $\delta$  of concentration polarization can vary from a few micrometers to hundreds of micrometers, depending on factors such as the nature of the feed solution, the design of the module, the transverse flow rate, and the transmembrane pressure (TMP). Three parameters define this model: the reflection coefficient  $\sigma$ , solute permeability  $P_s$ , and the thickness of the boundary layer  $\delta$ .

This study investigates the influence of initial nitrate concentration (IC) in real groundwater and TMP on nitrate rejection through NE90 and RE-BN membranes. Three mathematical models are utilized to explore the impact of nitrate IC on its transportation through the NE90 nanofiltration membrane and the RE-BN reverse osmosis membrane.

To analyze the contributions of diffusive and convective transfer to nitrate transport in the two membranes, both the KK and SK models are employed. However, these models do not account for the influence of the concentration polarization layer (CP) and electrical effects. The parameters of these models ( $C_{conv}$ ,  $J_{diff}$ ,  $P_s$ , and  $\sigma$ ) are calculated under different IC conditions. The third model, NP-FT, is used to predict nitrate rejection and determine the thickness of the concentration polarization layer ( $\delta$ ) at different IC.

## 2. Materials and methods

### 2.1. Feed water

The water used as the feed solution is a groundwater from the Mnasra, Gharb Region (Morocco) spiked at different concentrations of nitrates (50, 100, 200, 300, 400 and 500 mg/L), prepared from  $\text{NaNO}_3$  reagent. Only a slight variation in pH and electric conductivity (EC) was observed. The feed water properties are given in Table 1.

### 2.2. Unit pilot used

The tests were conducted using a NF/RO pilot plant (E 3039) provided by the French Company TIA (Fig. 1). The applied TMP varied between 5 and 70 bar. The pilot plant consists of two identical pressure vessels arranged in series, with each vessel housing one element. There is a pressure loss of approximately 2 bar, with each pressure vessel accounting for one bar. Both spiral-wound modules are outfitted with identical commercial membranes. To keep a constant temperature of 29°C, a heat exchanger is employed.

Table 1  
Physico-chemical composition of water doped with  $\text{NaNO}_3$

Nitrate (mg/L)	50	100	200	300	400
pH	8.2	8.19	8.18	8.2	8.21
EC ( $\mu\text{S}/\text{cm}$ )	1,902	1,913	1,921	1,926	1,932
$\text{Mg}^{2+}$ (mg/L)	42	42	42	42	42
$\text{Ca}^{2+}$ (mg/L)	145	145	145	145	145
$\text{Cl}^-$ (mg/L)	188	188	188	188	188
$\text{SO}_4^{2-}$ (mg/L)	158	158	158	158	158

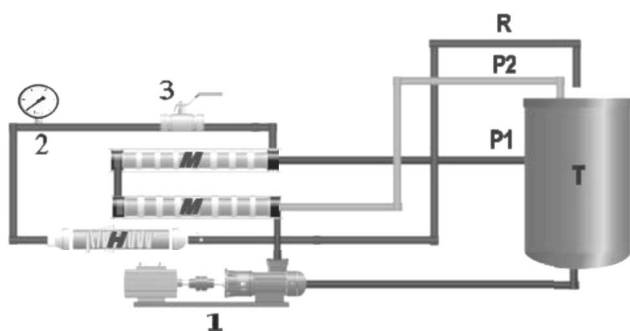


Fig. 1. Schematic diagram of the NF/RO pilot plant. T: tank; M: NF/RO module; P: permeate recirculation; R: retentate recirculation; H: heat exchanger; 1: high-pressure pump; 2: pressure sensor; 3: pressure regulation valves.

The water to be processed is pumped from the tank and introduced into the initial vessel. Subsequently, the retentate is directed into the second vessel, and the two resulting permeates are collected and combined. In addition, the membrane must be cleaned and rinsed each time the demineralization performance is impaired (fouling) and after each test cycle to restore the initial conditions before processing another solution again. The cleaning process should be performed in one of the following cases:

- Appearance of a precipitate in the brine or hydraulic circuits;
- Shutdown for more than a day.

To clean the pilot membrane stack, an alternate circulation of dilute acid (pH = 3) and basic solutions (pH = 11) is recommended, preceded and followed by flushing with water.

### 2.3. Membranes tested

The two spiral wound modules are equipped with two identical commercial NF membranes. Table 2 gives the characteristics of the membranes used.

### 2.4. NF/RO flux and rejection

The performance of the two membranes is measured in terms of rejection  $R$  and flux  $J_v$  by Eq. (1):

$$R\% = \left( 1 - \frac{C_p}{C_f} \right) \times 100 \quad (1)$$

where  $C_p$  (mg/L) and  $C_f$  (mg/L) are the permeate and feed concentrations, respectively.

$$J_v = \frac{V}{t \times A} \quad (2)$$

where  $V$  (L) is the volume of permeate collected in a given time interval  $t$  (h) and  $A$  is the membrane area ( $\text{m}^2$ ).

## 3. Results and discussion

### 3.1. Influence of operating variables

Fig. 2 gives, for the membranes tested, the variations of the average flux, EC and the permeate concentration as a function of TMP.

The results indicate that the permeate flux increases linearly with increasing TMP for both membranes, in accordance with Darcy's law (Fig. 2a). However, the flux obtained by NF is higher than that obtained by RO, likely due to NF being more porous than RO. A recent study published by Richards et al. [56] shows that there will be a drop in water flux at high applied pressure using polyamide and cellulose triacetate RO membranes. This drop of water permeance was observed at pressures below 50 bar, whereas the solution diffusion (SD) model predicts the onset of flux decline at pressures above ~400 bar. This study revealed that water travels in clusters through transiently connected

Table 2  
Characteristics of the membranes used

Membrane	NE90	RE-BN
Manufacture	CSM	CSM
Technic	Nanofiltration	Reverse osmosis
Cut-off	200D	–
Geometry	Spiral	Spiral
Effective membrane area	7.9 m <sup>2</sup>	7 m <sup>2</sup>
Membrane type	Thin-film composite	Thin-film composite
Membrane material	Polyamide (PA)	Polyamide (PA)
Permeate flow rate	6.4 m <sup>3</sup> /d	7.6 m <sup>3</sup> /d
NaCl rejection	90%–97%	99.4%

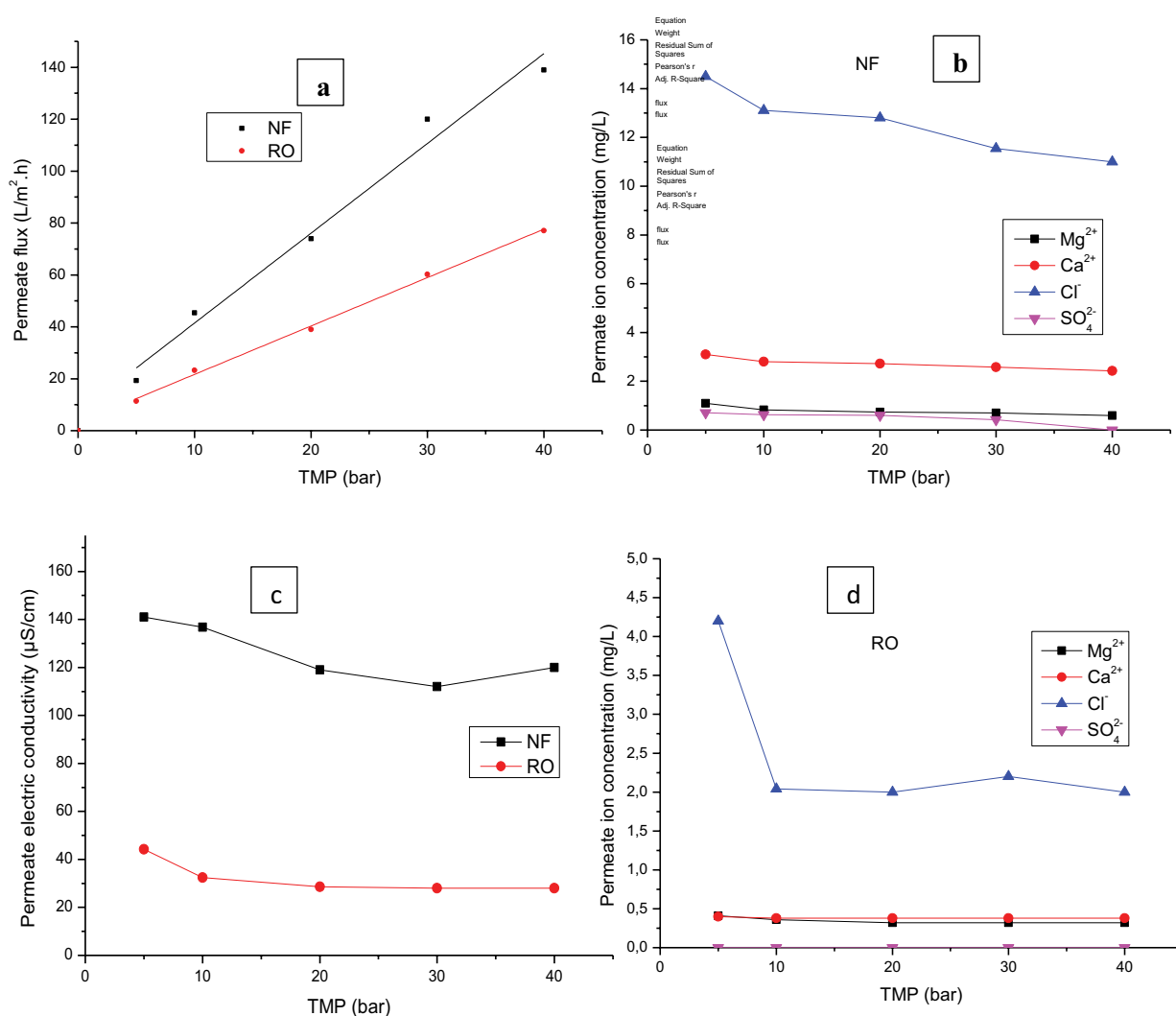


Fig. 2. Permeate characteristics as a function of operating TMP. (a) Permeate flux vs. TMP, (b) permeate ion concentration for NF membrane vs. TMP, (c) permeate electric conductivity vs. TMP, and (d) permeate ion concentration for RO membrane vs. TMP.

pores or free volumes inside the polyamide membrane under a pressure gradient. Moreover, they found that the solvent permeance depends also on the molecular size of the solvent rather than on the solubility of the solvent contrary to the classical model of SD.

The values of ion contents and EC in the NF permeate are slightly higher than those obtained in RO permeate, but still well below WHO standards. The behavior of the two membranes is similar, as the NF cut-off is very low and close to that of RO membranes (Fig. 2b–d).

The impact of TMP at various nitrate concentrations on nitrate rejection is depicted in Fig. 3. The findings show that the RE-BN membrane displays greater nitrate rejection compared to the NE90 membrane. A study conducted by Paugam et al. [57] revealed that the type of membrane influences nitrate rejection, greater rejection was observed with tighter membranes. The transfer of this ion is contingent upon both charge and steric exclusion. The results show that the rejection of nitrate increases with rising TMP before stabilizing for both membranes. Kedem [58] in their study, explains this increase in rejection as a function of pressure followed by its stabilization at a plateau by at pressure rises, surface forces remain consistent, but drag forces escalate due to the pore flux. At low pressure, surface forces exert more influence than drag forces. As a result, the cation flux (and consequently the nitrate flux necessary to maintain electroneutrality) stays low, while the solvent flux continues to rise with pressure. This results in an elevation of solute rejection. Beyond a certain pressure threshold, drag forces surpass surface forces. Consequently, solute transfer increases, leading to a reduction in rejection or its stabilization as a plateau.

### 3.2. Mathematical models

To comprehend the nitrate ion transfer mechanism and assess the roles of convective and diffusive transfers in the two examined membranes, three mathematical models are employed. The KK and SK models disregard the impact of the concentration polarization layer (CP) and electrostatic interactions, while the NP-FT model considers the CP but omits the electrical effects.

### 3.3. KK model

According to this model, the solute flux is a combination of two components: diffusion and convection. Typically, the concentration disparity between the membrane and the permeate drives diffusive transport, whereas convection results from the pressure gradient across the membrane [59]. The KK model introduced Eq. (3) to assess the

contributions of convection and diffusion in the process of solute mass transport within the examined membranes [60].

$$J_{\text{diff}} + J_v C_{\text{conv}} = C_p J_v \quad (3)$$

Eq. (1) can be expressed as follows:

$$C_p = \frac{J_{\text{diff}}}{J_v} + C_{\text{conv}} \quad (4)$$

where  $J_v$ : solvent flux (L/m<sup>3</sup>·h);  $C_p$ : concentration in permeate (mg/L);  $J_{\text{diff}}$ : diffusional flux (L/m<sup>3</sup>·h);  $C_{\text{conv}}$ : convective concentration (mg/L).

Eq. (4) is a straight line, which gives the variation of the concentration in the permeate as a function of the inverse of the permeate flux. The intercept gives the concentration in the permeate due to convection  $C_{\text{conv}}$  and the slope gives the flux of solute transported by diffusion  $J_{\text{diff}}$ .

Fig. 4 shows the variation of the nitrate concentration in the permeate  $C_p$  as a function of the inverse of the permeate flux  $1/J_p$  and Table 3 gives the values of  $C_{\text{conv}}$ ,  $J_{\text{diff}}$  and  $R$ -square obtained.

Fig. 4 demonstrates an acceptable accuracy of the linear relationship between  $C_p$  and  $1/J_p$ , as per Eq. (4). The  $C_{\text{conv}}$  and  $J_{\text{diff}}$  of the NE90 membrane are higher than those of the RE-BN membrane. This is due to the NE90 membrane being more porous and sensitive to the initial nitrate concentration than the RE-BN membrane, resulting in greater flux and solute passage in the permeate. These findings indicate that both the NE90 and RE-BN membranes involve two distinct transfer mechanisms (diffusional and convective) that operate independently, but additively in the overall transfer process.

The impact of the IC of nitrate on the convective concentration and diffusion flux for both membranes is examined and depicted in Fig. 5. The results reveal that the changes in the convective concentration and diffusion flux of nitrate ions, as a function of IC are accurately represented by a linear relationship with an  $R$ -squared value greater than 0.86 for both membranes. The convective

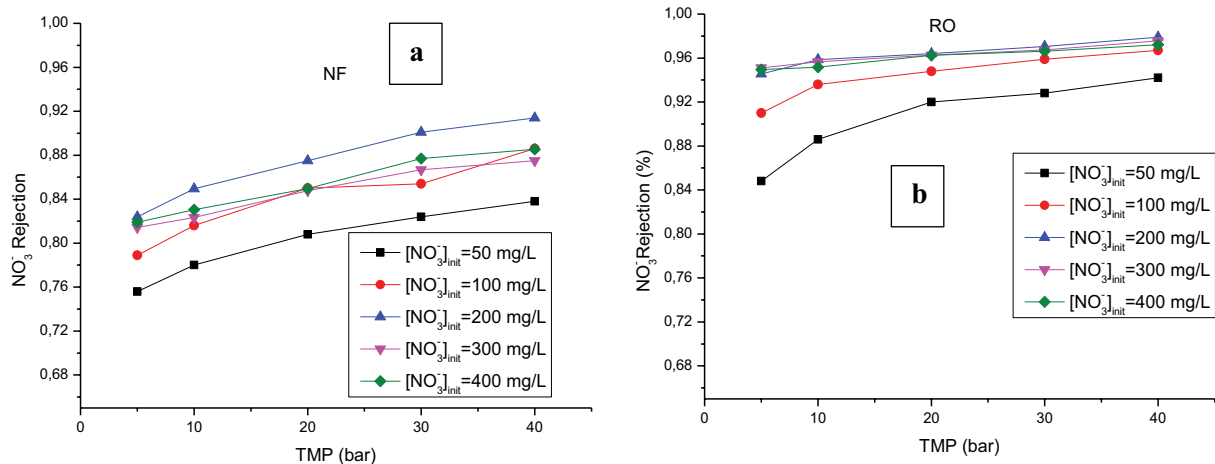


Fig. 3. Nitrate rejection vs. TMP. (a) Nitrate rejection on different feed nitrate concentrations vs. TMP for NF membrane. (b) Nitrate rejection on different feed nitrate concentrations vs. TMP for RO membrane.

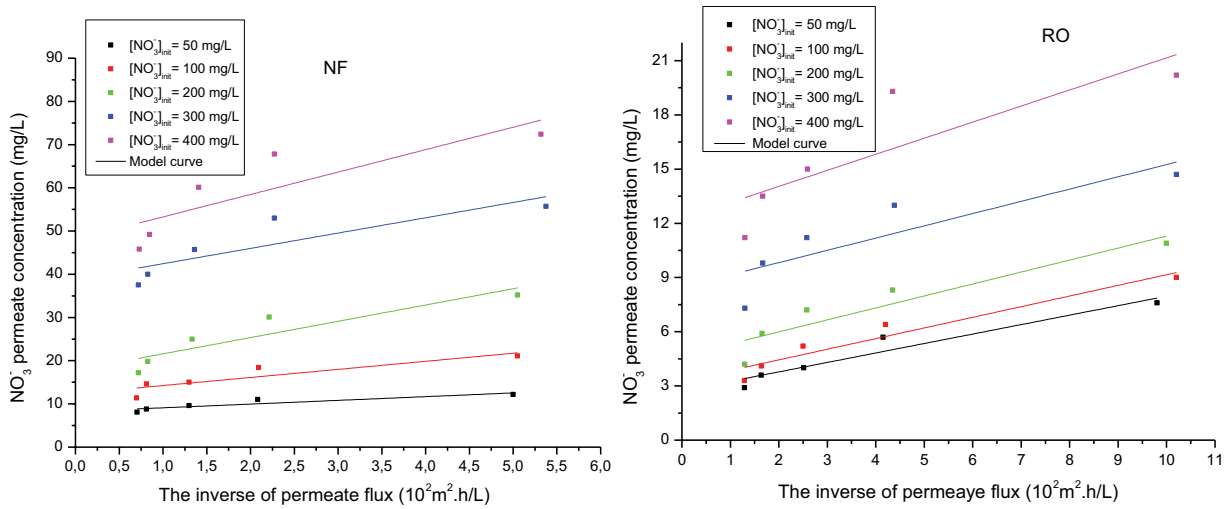


Fig. 4. Permeate concentration of nitrate as a function of the inverse of the permeate flux, for different initial feed concentrations.

Table 3  
 $C_{conv}$  and  $J_{diff}$  values obtained at different initial feed concentration of nitrate

Initial feed concentration		50 mg/L	100 mg/L	200 mg/L	300 mg/L	400 mg/L
NF	$C_{conv}$ (mg/L)	8.2334	12.17	17.823	38.91	48.09
	$J_{diff}$	86.17	186.96	376.51	354.262	518.67
	R-square	0.80	0.75	0.79	0.66	0.64
RO	$C_{conv}$ (mg/L)	2.73	3.262	4.67	8.47	12.264
	$J_{diff}$	52.36	58.92	66.242	67.81	88.93
	R-square	0.91	0.92	0.84	0.67	0.63

concentration and diffusion flux of nitrate ions increase with increasing IC for both membranes, with a more significant increase observed in the case of the NE90 membrane. This increase in IC of nitrate causes the increase concentration between the feed side and the permeate side of the membrane. This difference in concentration creates an osmotic gradient, that is, an osmotic pressure difference; as a result, solutes are further pushed across the membrane by convective transport, resulting in a linear increase in convective concentration with increasing initial concentration in the feed. This linear behavior may be governed by the laws of fluid mechanics. On the other hand, diffusion is a phenomenon that occurs naturally when molecules move from an area of high concentration to an area of lower concentration. By increasing the IC of nitrate, the concentration gradient increases, which means that solutes will have faster and more sustained movement across the membrane and hence increased diffusive flux. The linear behavior conforms to Fick’s law, which mathematically describes the diffusion of solutes. According to this law, the diffusion flux is directly proportional to the concentration gradient.

3.4. SK model

The KK model lacks the capability to differentiate between the contributions of convective and diffusive solute

transfers, leading to the utilization of the SK model, which not only enables such differentiation but also permits the quantification of solute permeability. The SK model is based on the principles of non-equilibrium thermodynamics, treating the membrane as a black box. This approach facilitates the characterization of membranes in terms of two key parameters: the reflection coefficient ( $\sigma$ ) and solute permeability ( $P_s$ ) [39,40].

From this postulate, it is then possible to express the solvent flux  $J_v$  and the solute flux  $J_s$  Eqs. (5) and (6):

$$J_v = L_p (\Delta P - \sigma \Delta \pi) \tag{5}$$

$$J_s = P_s (C_m - C_p) + (1 - \sigma) J_v C_m \tag{6}$$

where  $L_p$ : membrane permeability to solvent ( $m^3/m^2 \cdot h$ );  $\Delta P$ : pressure (bar);  $\sigma$ : reflection coefficient of the solute by the membrane;  $C_m$ : concentration at the membrane surface (mg/L);  $\Delta \pi$ : osmotic pressure due to the solute (bar);  $P_s$ : permeability of the solute ( $m^3/m^2 \cdot h$ ).

The real rejection can be calculated by this theory for species “i” Eq. (7):

$$R = 1 - \frac{C_p}{C_f} = \frac{\sigma(1-F)}{1-\sigma F} \quad \text{where } F = \exp\left(\frac{(1-\sigma)J_v}{P_s}\right) \tag{7}$$

The experimental nitrate rejection was modulated using Eq. (7) from the SK model to investigate the impact of the initial concentration (IC) on both the contribution of each transfer mechanism (convective and diffusive) and the phenomenological parameter ( $\sigma$ ,  $P_s$ ) in ion transport within the examined membranes. The variation of nitrate rejection at different IC is illustrated in Fig. 6, demonstrating a good agreement between the experimental and fitted results obtained through the SK model for both membranes. The results obtained are collected in Table 4.

As summarized in Table 4, the high values of  $R$ -square that exceed 0.99 shows a good fit of the model and experimental results. In addition, the values of  $\sigma$  and  $P_s$  found are of the same order as the results obtained by NF and RO in our previous paper for the rejection of nitrates from a real brackish water. These values of  $\sigma$  and  $P_s$  for the membrane NE90 were 0.94 and  $7.45 \times 10^{-7}$  m/s, respectively, and 0.98 and  $8.92 \times 10^{-8}$  m/s, respectively for RO membrane BW30 [52]. According to the obtained values of  $\sigma$ , the NE90 membrane is more convective than the RE-BN membrane and that the transfer of nitrates by diffusion in these two membranes is predominant.

The effect of the IC of nitrate on the calculated transport parameters ( $\sigma$ ,  $P_s$ ) is investigated for both membranes as shown in Fig. 7. The results show a linear behavior of permeability of nitrate for both membranes. This permeability decreases with increasing IC for both membranes. For RE-BN membrane, when the IC increases from 50 to 400 mg/L, permeability of nitrate decreases linearly from 4.01 to 0.936 m/s $\cdot$ 10 $^{-7}$ , which represents a drop of 23.34%. For NE90, permeability of nitrate decreases linearly from 9.51 to 6.57 m/s $\cdot$ 10 $^{-7}$ , which represents a drop of 69.08%. View that nitrate transfer by diffusion for both membranes is dominant, increasing the IC of nitrate creates a larger concentration gradient across the membrane. As a result, the driving force for the diffusion of nitrate across the membrane becomes stronger, resulting in a decrease in permeability of nitrate. This result is consistent with the increase in reflection coefficient as a function of IC. The phenomenological parameters in this model ( $\sigma$  and  $P_s$ ) exhibit dependency on IC of nitrate with a more significant dependence observed in the case of the NE90 membrane. Higher IC of nitrate promote more efficient selective diffusion across both membranes.

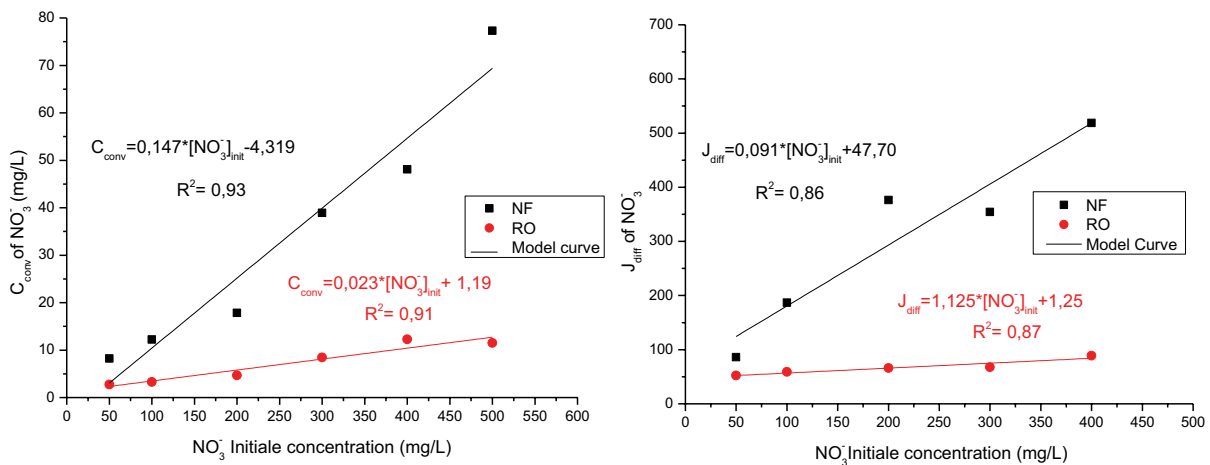


Fig. 5. Variation  $J_{diff}$  (a) and convective concentration  $C_{conv}$  (b) of nitrate as a function of IC of nitrate.

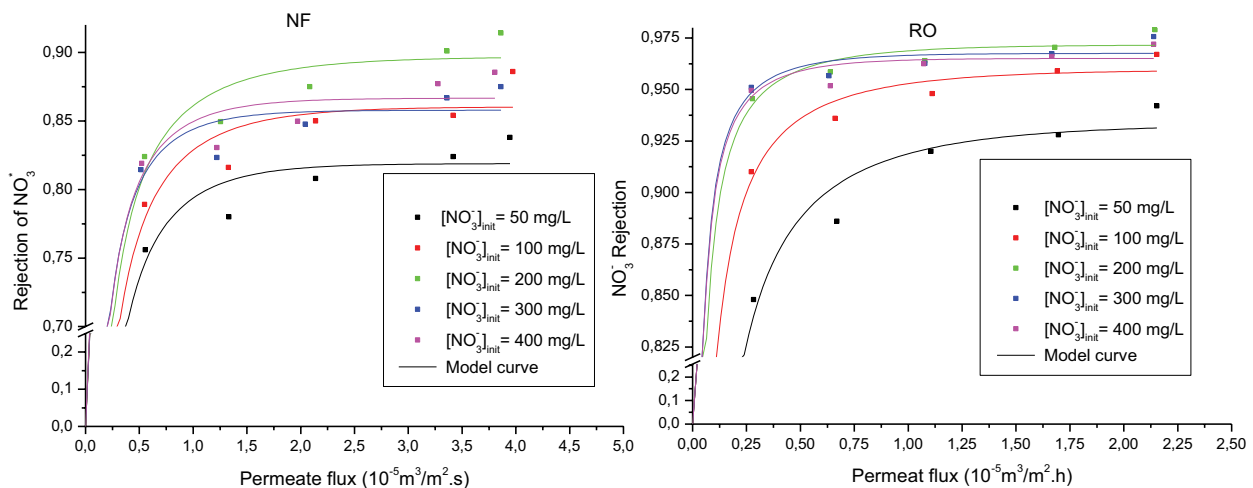


Fig. 6. Experimental and fitting data of nitrate rejection as a function of permeate flux for NE90 and RE-BN membranes.

Table 4  
Calculated values of  $\sigma$  and  $P_s$  by Spiegler–Kedem model

Initial feed concentration (mg/L)		50	100	200	300	400
NF	$P_s (\text{m}^3/\text{m}^2 \cdot \text{s}) \times 10^{-7}$	9.50	9.07	8.25	6.27	6.56
	$\sigma$	0.81	0.86	0.89	0.85	0.86
	R-square	0.997	0.996	0.997	0.997	0.997
RO	$P_s (\text{m}^3/\text{m}^2 \cdot \text{s}) \times 10^{-7}$	4.01	2.12	2.12	0.924	0.936
	$\sigma$	0.933	0.959	0.959	0.967	0.965
	R-square	0.999	0.999	0.999	0.999	0.999

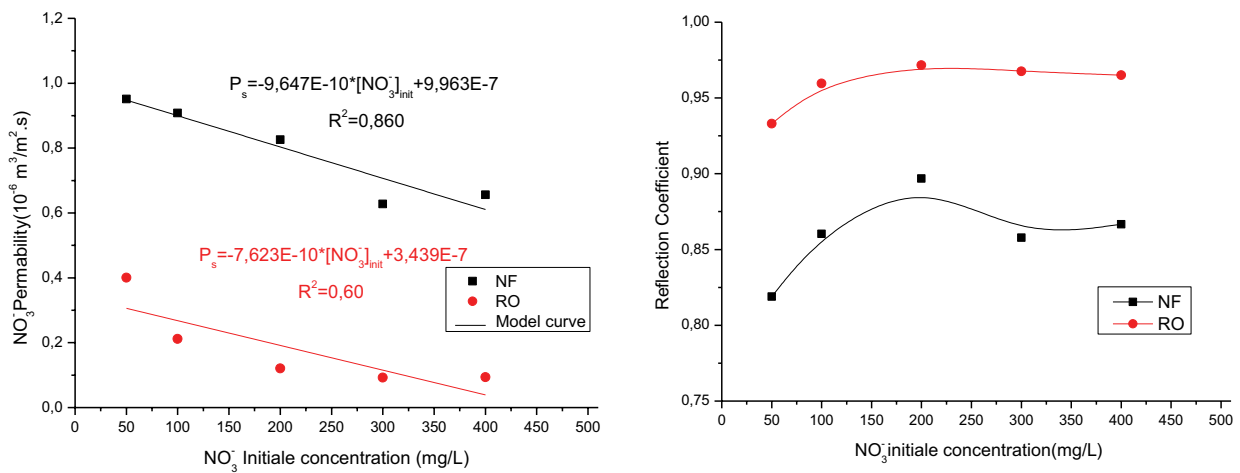


Fig. 7. Permeability of nitrate and reflection coefficient as a function of IC of nitrate for NE90 and RE-BN membranes.

3.5. Nernst–Planck modeling coupled with film theory

To account for the effect of the concentration polarization layer on the  $P_s$  and the  $\sigma$  at different nitrate ICs, the NP-FT model is used for both membranes.

The transport equation for species  $i$  can be described by the simplified extended Nernst–Planck given by Dresner [60]:

$$J_i = -P \left( \frac{dC_i}{dx} + \frac{C_i F z_i}{RT} \frac{d\phi}{dx} \right) + J_v C_i (1 - \sigma) \tag{8}$$

where  $P$  ( $\text{m}^2/\text{s}$ ) and  $s$  are the parameters of SK model;  $C_i$ : ion concentration (mg/L);  $d\phi$ : Donnan potential (V);  $z_i$ : ion valence;  $F$ : Faraday constant (C/mol).

Rearrangement of Eq. (6), written for a binary system, containing species 1 and 2, together with electroneutrality conditions.

$$\sum i C_i z_i = 0 \tag{9}$$

$$\sum i C_i J_i = 0 \tag{10}$$

$$J_i = -P \frac{dC_i}{dx} + J_v C_i (1 - \sigma) \tag{11}$$

The Spiegler–Kedem equation, is integrated over the thickness of membrane ( $0 < x < \Delta x$ ) using the following boundary conditions:

$$C_i = C_{mi} \text{ at } x = 0;$$

$$C_i = C_{pi} \text{ at } x = \Delta x.$$

and

$$J_i = C_{pi} J_v \tag{12}$$

The solution is:

$$C_{mi} = \left\{ 1 - \frac{\sigma}{\exp \left[ (1 - \sigma) \frac{J_v}{P_s} \right]} \right\} \frac{C_{pi}}{1 - \sigma} \tag{13}$$

where  $P_s = P/\Delta x$ .

If a concentration polarization is assumed to occur within a boundary layer adjacent to membrane/feed solution interface, at steady state the following mass balance can be constructed:

$$J_v C_{pi} = J_v C_{mi} - D \frac{dC_i}{dx} \quad (14)$$

Integration of Eq. (14) over the thickness of boundary layer:

$$\frac{C_{mi} - C_{pi}}{C_{fi} - C_{pi}} = \exp\left(\frac{\delta}{D} J_v\right) \quad (15)$$

Then  $C_{mi}$  is given by:

$$C_{mi} = C_{pi} - (C_{pi} - C_{fi}) \exp\left(\frac{\delta}{D} J_v\right) \quad (16)$$

The Eq. (13) is then equal to Eq. (16) so:

$$\frac{C_{pi}}{C_{fi}} = \frac{1}{1 + \frac{\sigma}{1 - \sigma} \left\{ \exp\left[-J_v \frac{\delta}{D}\right] - \exp\left[-\frac{(1 - \sigma) J_v}{P_s} - \frac{J_v \delta}{D}\right] \right\}} \quad (17)$$

Finally, the rejection of ion “i” can then be written as:

$$R_i = 1 - \frac{C_{pi}}{C_{fi}} = 1 - \frac{1}{1 + \frac{\sigma}{1 - \sigma} \left\{ \exp\left[-J_v \frac{\delta}{D}\right] - \exp\left[-\frac{(1 - \sigma) J_v}{P_s} - \frac{J_v \delta}{D}\right] \right\}} \quad (18)$$

The NP-FT model is utilized to investigate the effect of (IC) of nitrate on reflection coefficient ( $\sigma$ ), solute permeability ( $P_s$ ), and boundary layer thickness ( $\delta$ ), while considering the phenomenon of concentration polarization. To achieve this, a Python program was developed based on the flowchart proposed by Chaabane et al. [54]. The simulation results generated from the model are used to produce the curves depicted in Fig. 8, where solid symbols represent experimental data, and solid lines represent the model function with parameters determined by the program using Eq. (18). The calculated model parameters are summarized in Table 5.

Fig. 8 demonstrates a favorable agreement between the experimentally obtained nitrate rejection and the NP-FT model's predictions for the studied membranes, across a

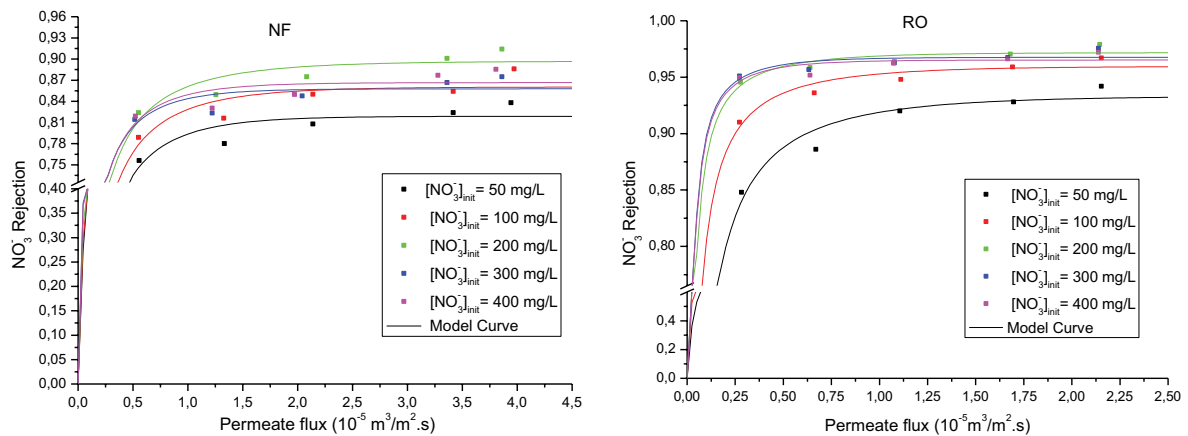


Fig. 8. Experimental and model data of nitrate rejection vs permeate flux for the three membranes.

Table 5  
Parameters,  $\sigma$ ,  $P_s$  and  $\delta$  obtained by the coupled NP-FT model

Membrane	IC (mg/L)	$P_s$	$\delta$ (m)	$\sigma$	$R^2$
NF	50	9.499E-07	1.041E-08	0.8189	0.9977
	100	9.198E-07	1.045E-08	0.8605	0.9974
	200	8.296E-07	1.026E-08	0.8959	0.9979
	300	6.737E-07	1.406E-08	0.8577	0.9979
	400	6.94E-07	1.42E-08	0.8662	0.9978
	Medium	7.3243E-07	1.406E-08	0.85984	0.99774
RO	50	4.868E-07	1.022E-12	0.9131	0.9977
	100	2.21E-07	1.026E-12	0.960	0.9997
	200	1.22E-07	1.228E-12	0.9716	0.9998
	300	9.588E-08	1.32E-12	0.9675	0.9998
	400	9.731E-08	1.03E-12	0.9651	0.9998
	Medium	2.04598E-07	1.1252E-12	0.95546	0.99936

range of nitrate ICs, as evidenced by the high  $R$ -squared values.

According to Table 5, the results obtained confirm those obtained by the SK model, concerning the permeability of nitrates and the mode of transfer. In addition, for the RE-BN membrane, the values of the permeability of nitrate ions are very low compared to those obtained by the NE90 membrane. This translates into a very low  $\delta$  for the RE-BN membrane which is of the order of  $10^{-12}$  m. In contrast, the order of magnitude of  $\delta$  for the NE90 membrane is  $10^{-8}$  m.

According to Table 5, the values of  $\delta$  do not appear to vary with nitrate concentration for both types of membranes. A recent study conducted by Lopez et al. [61] yielded similar results using a solution-electro-diffusion-film coupled reactive transport (SEDFRT) model to describe solute transport through NF270 membranes in complex multi-electrolyte environments (strong and weak). They estimated a  $\delta$  value for NF270 in the order  $10^{-7}$  m, which is slightly larger compared to the  $\delta$  values of NE90 and RE-BN.

#### 4. Conclusion

In order to investigate and characterize nitrate transport through NF and RO membranes, three different transport models are employed. These models are evaluated for six different IC of nitrate and for both the NE90 and RE-BN membranes.

The KK model is utilized to analyze the diffusive and convective transport of the NE90 and RE-BN membranes. The model's findings demonstrate a favorable concurrence between the experimental and fitting results for both membranes. The KK model demonstrates that the two membranes have distinct transfer mechanisms, which act independently but contribute to the overall transfer additively. The  $C_{\text{conv}}$  and  $J_{\text{diff}}$  parameters of the NE90 membrane are significantly influenced by the IC of nitrate, whereas those of the RE-BN membrane are only mildly impacted.

To calculate nitrate transport, the SK model is utilized. At the same time, the two parameters  $P_s$  and  $\sigma$  are determined. The results of SK model exhibit a good agreement between the experimental and fitting outcomes for both membranes. In addition, it shows that for nitrate ions the transfer by diffusion is dominant for both membranes. It is observed that the two parameters of the model are dependent on IC of nitrate. The dependence of  $P_s$  and  $\sigma$  on the IC of nitrate is more marked for the nanofiltration membrane than for the reverse osmosis membrane.

The Nernst–Planck model coupled with film theory is an adequate description for mass transport through both NF and RO membranes due to its consideration of concentration polarization. The experimental nitrate rejection results show a good fit with the NP-FT model. Additionally, the model indicates that the  $\delta$  of CP of nitrate is negligible for the RO membrane and on the order of  $10^{-8}$  m for the NF membrane.

#### References

- [1] E. Abascal, L. Gómez-Coma, I. Ortiz, A. Ortiz, Global diagnosis of nitrate pollution in groundwater and review of

- removal technologies, *Sci. Total Environ.*, 810 (2022) 152233, doi: 10.1016/J.SCITOTENV.2021.152233.
- [2] B. Bishayee, R.P. Chatterjee, B. Ruj, S. Chakraborty, J. Nayak, Strategic management of nitrate pollution from contaminated water using viable adsorbents: an economic assessment-based review with possible policy suggestions, *J. Environ. Manage.*, 303 (2022) 114081, doi: 10.1016/J.JENVMAN.2021.114081.
- [3] F. da Silva Peixoto, I.N. Cavalcante, D.F. Gomes, Influence of land use and sanitation issues on water quality of an urban aquifer, *Water Resour. Manage.*, 34 (2020) 653–674.
- [4] Y. Boudjana, S. Brouyère, P. Jamin, P. Orban, D. Gasparella, A. Dassargues, Understanding groundwater mineralization changes of a Belgian chalky aquifer in the presence of 1,1,1-trichloroethane degradation reactions, *Water*, 11 (2019) 2009, doi: 10.3390/W11102009.
- [5] M. Barbieri, L. Ricolfi, S. Vitale, P.V. Muteto, A. Nigro, G. Sappa, Assessment of groundwater quality in the buffer zone of Limpopo National Park, Gaza Province, Southern Mozambique, *Environ. Sci. Pollut. Res.*, 26 (2018) 62–77.
- [6] N. El Khodrani, S. Omrania, A. Nouayti, A. Zouahri, A. Douaik, H. Iaaich, M. Lahmar, M. Fekhaoui, Comparative study of groundwater pollution of M'nasra and Sfaafa zones (Charb, Morocco) by nitrates, *E3S Web Conf.*, 150 (2020) 01006, doi: 10.1051/E3SCONF/202015001006.
- [7] S. Kamal, S. Sefiani, N.E. Laftouhi, A. El Mandour, J. Moustadraf, M. Elgettafi, M. Himi, A. Casas, Hydrochemical and isotopic assessment for characterizing groundwater quality and recharge processes under a semi-arid area: case of the Haouz plain aquifer (Central Morocco), *J. Afr. Earth Sci.*, 174 (2021) 104077, doi: 10.1016/J.JAFREARSCI.2020.104077.
- [8] S. Omrania, N. El Khodrani, A. Zouahri, A. Douaik, H. Iaaich, M. Lahmar, S. El Hajjaji, Evaluation of the groundwater quality of the M'nasra, Kenitra (Morocco), *Mater. Today Proc.*, 13 (2019) 1092–1101.
- [9] M.F. Abu-Alnaeem, I. Yusoff, T.F. Ng, Y. Alias, M. Raksmei, Assessment of groundwater salinity and quality in Gaza Coastal Aquifer, Gaza Strip, Palestine: an integrated statistical, geostatistical and hydrogeochemical approaches study, *Sci. Total Environ.*, 615 (2018) 972–989.
- [10] S. Jehan, S. Khan, S.A. Khattak, S. Muhammad, A. Rashid, N. Muhammad, Hydrochemical properties of drinking water and their sources apportionment of pollution in Bajaur Agency, Pakistan, *Measurement*, 139 (2019) 249–257.
- [11] M. Kumari, S.C. Rai, Hydrogeochemical evaluation of groundwater quality for drinking and irrigation purposes using water quality index in semi-arid region of India, *J. Geol. Soc. India*, 95 (2020) 159–168.
- [12] H. Feng, S. Dong, Y. Li, H. Hu, T. Zhang, Z. Li, B. Liu, Characterizing nitrogen distribution, source and transformation in groundwater of ecotone of agriculture–animal husbandry: an example from North China, *Environ. Earth Sci.*, 79 (2020) 1–16.
- [13] M. Gutiérrez, R.N. Biagioni, M.T. Alarcón-Herrera, B.A. Rivas-Lucero, An overview of nitrate sources and operating processes in arid and semiarid aquifer systems, *Sci Total Environ.*, 624 (2018) 1513–1522.
- [14] G. Tokazhanov, E. Ramazanov, S. Hamid, S. Bae, W. Lee, Advances in the catalytic reduction of nitrate by metallic catalysts for high efficiency and  $N_2$  selectivity: a review, *Chem. Eng. J.*, 384 (2020) 123252, doi: 10.1016/J.CEJ.2019.123252.
- [15] N. Khatri, S. Tyagi, D. Rawtani, Assessment of drinking water quality and its health effects in rural areas of Harij Taluka, Patan District of Northern Gujarat, *Environ. Claims J.*, 28 (2016) 223–246.
- [16] A. Bhatnagar, M. Sillanpää, A review of emerging adsorbents for nitrate removal from water, *Chem. Eng. J.*, 168 (2011) 493–504.
- [17] X. Zhang, Y. Zhang, P. Shi, Z. Bi, Z. Shan, L. Ren, The deep challenge of nitrate pollution in river water of China, *Sci. Total Environ.*, 770 (2021) 144674, doi: 10.1016/J.SCITOTENV.2020.144674.
- [18] A. Boubakri, A. Hafiane, S. Al Tahar Bouguecha, Nitrate removal from aqueous solution by direct contact membrane

- distillation using two different commercial membranes, *Desal. Water Treat.*, 56 (2014) 2723–2730.
- [19] World Health Organization, Nitrate and Nitrite in Drinking Water, Background Document for Development of WHO Guidelines for Drinking Water Quality, Background Document for Development of WHO Guidelines for Drinking Water Quality, 2017. Available at: <http://www.who.int/publications/guidelines/> (Accessed November 12, 2020).
- [20] NM 03.7.001, Norme marocaine relative à la qualité des eaux d'alimentation humaine, Bulletin Officiel N° 5404, 16 Mars 2006.
- [21] F. Elhannouni, M. Belhadj, M. Taky, L. Echihabi, M. Hafsi, H. El Abbassi, A.T. Cherif, A. El Midaoui, Denitrification of ground water by electrodialysis using a new anion exchange membrane, *J. Water Supply Res. Technol. AQUA*, 49 (2000) 211–218.
- [22] A. Elmidaoui, F. Elhannouni, M.A. Menkouchi Sahli, L. Chay, H. Elabbassi, M. Hafsi, D. Largeteau, Pollution of nitrate in Moroccan ground water: removal by electrodialysis, *Desalination*, 136 (2001) 325–332.
- [23] M.A. Menkouchi Sahli, M. Tahaikt, I. Achary, M. Taky, F. Elhanouni, M. Hafsi, M. Elmghari, A. Elmidaoui, Technical optimisation of nitrate removal from ground water by electrodialysis using a pilot plant, *Desalination*, 167 (2004) 359, doi: 10.1016/j.desal.2004.06.146.
- [24] A. Elmidaoui, M.A. Menkouchi Sahli, M. Tahaikt, L. Chay, M. Taky, M. Elmghari, M. Hafsi, Selective nitrate removal by coupling electrodialysis and a bioreactor, *Desalination*, 153 (2003) 389–397.
- [25] S. Ebrahimi, D.J. Roberts, Sustainable nitrate-contaminated water treatment using multi cycle ion-exchange/bioregeneration of nitrate selective resin, *J. Hazard. Mater.*, 262 (2013) 539–544.
- [26] B.U. Bae, Y.H. Jung, W.W. Han, H.S. Shin, Improved brine recycling during nitrate removal using ion exchange, *Water Res.*, 36 (2002) 3330–3340.
- [27] B.U. Bae, Y.H. Jung, W.W. Han, H.S. Shin, H. Dong, C.S. Shepsko, M. German, A.K. Sengupta, Improved brine recycling during nitrate removal using ion exchange, *J. Environ. Chem. Eng.*, 8 (2002) 103846, doi: 10.1016/S0043-1354(02)00012-X.
- [28] M.I.M. Soares, Biological denitrification of groundwater, *Water Air Soil Pollut.*, 123 (2000) 183–193.
- [29] T. Kodera, S. Akizuki, T. Toda, Formation of simultaneous denitrification and methanogenesis granules in biological wastewater treatment, *Process Biochem.*, 58 (2017) 252–257.
- [30] R. Epsztein, O. Nir, O. Lahav, M. Green, Selective nitrate removal from groundwater using a hybrid nanofiltration–reverse osmosis filtration scheme, *Chem. Eng. J.*, 279 (2015) 372–378.
- [31] S. Tyagi, D. Rawtani, N. Khatri, M. Tharmavaram, Strategies for nitrate removal from aqueous environment using nanotechnology: a review, *J. Water Process Eng.*, 21 (2018) 84–95.
- [32] S.V. Jadhav, K.V. Marathe, V.K. Rathod, A pilot scale concurrent removal of fluoride, arsenic, sulfate and nitrate by using nanofiltration: competing ion interaction and modelling approach, *J. Water Process Eng.*, 13 (2016) 153–167.
- [33] S. El-Ghizel, H. Jalte, H. Zeggar, M. Zait, S. Belhamidi, F. Tiyal, M. Hafsi, M. Taky, A. Elmidaoui, Autopsy of nanofiltration membrane of a decentralized demineralization plant, *Membr. Water Treat.*, 10 (2019) 277–286.
- [34] S. El-Ghizel, H. Zeggar, M. Tahaikt, F. Tiyal, A. Elmidaoui, M. Taky, Nanofiltration process combined with electrochemical disinfection for drinking water production: feasibility study and optimization, *J. Water Process Eng.*, 36 (2020) 101225, doi: 10.1016/j.jwpe.2020.101225.
- [35] S. El-Ghizel, H. Zeggar, F. Elazhar, M. Tahaikt, M. Hafsi, A. Elmidaoui, M. Taky, Brine recycling impact on nitrate removal and electrochemical disinfection performances: a case study of Sidi Taibi desalination plant, *Desal. Water Treat.*, 240 (2021) 63–74.
- [36] J. Touir, S. El-Ghizel, H. Zeggar, S. Belhamidi, F. Elazhar, M. Tahaikt, M. Taky, A. Elmidaoui, Nanofiltration and reverse osmosis membrane for nitrate removal: performance study and economic evaluation, *Moroccan J. Chem.*, 9 (2021) 57–68.
- [37] S. El-Ghizel, H. Jalté, B. Bachiri, A. Zdeg, F. Tiyal, M. Hafsi, M. Taky, A. Elmidaoui, Demineralization of underground water by a nanofiltration plant coupled with a photovoltaic and wind energy system, *Desal. Water Treat.*, 130 (2018) 28–36.
- [38] F.H. Silva, S. Karakus, B. Musicki, H. Matsui, T.J. Bivalacqua, J.L. dos Santos, F.F. Costa, A.L. Burnett, Beneficial effect of the nitric oxide donor compound 3-(1,3-dioxoisindolin-2-yl) benzyl nitrate on dysregulated phosphodiesterase 5, NADPH Oxidase, and Nitrosative Stress in the Sickle Cell Mouse Penis: Implication for Priapism Treatment, *J. Pharm. Exp. Ther.*, 359 (2016) 230–237.
- [39] H. Al-Zoubi, N. Hilal, N.A. Darwish, A.W. Mohammad, Rejection and modelling of sulphate and potassium salts by nanofiltration membranes: neural network and Spiegler–Kedem model, *Desalination*, 206 (2007) 42–60.
- [40] O. Kedem, A. Katchalsky, Permeability of composite membranes. Part 1.—Electric current, volume flow and flow of solute through membranes, *Trans. Faraday Soc.*, 59 (1963) 1918–1930.
- [41] M. Da, B. Zheng, G. Lin, M.L. Sushko, Numerical solution of 3D Poisson–Nernst–Planck Equations coupled with classical density functional theory for modeling ion and electron transport in a confined environment, *Commun. Comput. Phys.*, 16 (2014) 1298–1322.
- [42] F.E. Ahmed, R. Hashaikeh, A. Diabat, N. Hilal, Mathematical and optimization modelling in desalination: state-of-the-art and future direction, *Desalination*, 469 (2019) 114092, doi: 10.1016/J.DESAL.2019.114092.
- [43] M. Soltanieh, W.N. Gill, Review of reverse osmosis membranes and transport models, *Chem. Eng. Commun.*, 12 (1981) 279–363.
- [44] A.W. Mohammad, N. Hilal, H. Al-Zoubi, N.A. Darwish, Prediction of permeate fluxes and rejections of highly concentrated salts in nanofiltration membranes, *J. Membr. Sci.*, 289 (2007) 40–50.
- [45] A. Ghorbani, B. Bayati, E. Drioli, F. Macedonio, T. Kikhavani, M. Frappa, Modeling of nanofiltration process using DSPM-DE model for purification of amine solution, *Membranes (Basel)*, 11 (2021) 230, doi: 10.3390/membranes11040230.
- [46] M.M. Zubair, H. Saleem, S.J. Zaidi, Recent progress in reverse osmosis modeling: an overview, *Desalination*, 564 (2023) 116705, doi: 10.1016/J.DESAL.2023.116705.
- [47] F. Wu, L. Feng, L. Zhang, Rejection prediction of isopropylantipyridine and antipyridine by nanofiltration membranes based on the Spiegler–Kedem–Katchalsky model, *Desalination*, 362 (2015) 11–17.
- [48] R.B. Merlet, C.R. Tanardi, I.F.J. Vankelecom, A. Nijmeijer, L. Winnubst, Interpreting rejection in SRNF across grafted ceramic membranes through the Spiegler–Kedem model, *J. Membr. Sci.*, 525 (2017) 359–367.
- [49] A.M. Hidalgo, G. León, M. Gómez, M.D. Murcia, E. Gómez, J.L. Gómez, Application of the Spiegler–Kedem–Kachalsky model to the removal of 4-chlorophenol by different nanofiltration membranes, *Desalination*, 315 (2013) 70–75.
- [50] S.R. Hosseinabadi, K. Wyns, V. Meynen, A. Buekenhoudt, B. van der Bruggen, Solvent-membrane-solute interactions in organic solvent nanofiltration (OSN) for Grignard functionalised ceramic membranes: explanation via Spiegler–Kedem theory, *J. Membr. Sci.*, 513 (2016) 177–185.
- [51] R.R. Nair, E. Protasova, S. Strand, T. Bilstad, Implementation of Spiegler–Kedem and steric hindrance pore models for analyzing nanofiltration membrane performance for smart water production, *Membranes (Basel)*, 8 (2018), doi: 10.3390/membranes8030078.
- [52] B. Cuartas-Urbe, M.C. Vincent-Vela, S. Álvarez-Blanco, M.I. Alcaina-Miranda, E. Soriano-Costa, Nanofiltration of sweet whey and prediction of lactose retention as a function of permeate flux using the Kedem–Spiegler and Donnan Steric Partitioning models, *Sep. Purif. Technol.*, 56 (2007) 38–46.
- [53] H. Zeggar, J. Touir, S. El-Ghizel, F. Elazhar, M. Tahaikt, D. Dhiba, A. Elmidaoui, M. Taky, Characterization of ion transfer and modelling of fouling in nanofiltration and

- reverse osmosis membranes, *Desal. Water Treat.*, (2021), doi: 10.5004/dwt.2021.27542.
- [54] T. Chaabane, S. Taha, M. Taleb Ahmed, R. Maachi, G. Dorange, Coupled model of film theory and the Nernst–Planck equation in nanofiltration, *Desalination*, 206 (2007) 424–432.
- [55] L. Wang, J. He, M. Heiranian, H. Fan, L. Song, Y. Li, M. Elimelech, Water transport in reverse osmosis membranes is governed by pore flow, not a solution–diffusion mechanism, *Sci. Adv.*, 9 (2023), doi: 10.1126/sciadv.adf8488.
- [56] L.A. Richards, M. Vuachère, A.I. Schäfer, Impact of pH on the removal of fluoride, nitrate and boron by nanofiltration/reverse osmosis, *Desalination*, 261 (2010) 331–337.
- [57] L. Paugam, S. Taha, G. Dorange, P. Jaouen, F. Quéméneur, Mechanism of nitrate ions transfer in nanofiltration depending on pressure, pH, concentration and medium composition, *J. Membr. Sci.*, 231 (2004) 37–46.
- [58] O. Kedem, Commentary on ‘thermodynamic analysis of the permeability of biological membranes to non-electrolytes’ by O. Kedem and A. Katchalsky, *Biochim. Biophys. Acta*, 27 (1958) 229–246.
- [59] X.L. Wang, T. Tsuru, S.I. Nakao, S. Kimura, The electrostatic and steric-hindrance model for the transport of charged solutes through nanofiltration membranes, *J. Membr. Sci.*, 135 (1997) 19–32.
- [60] L. Dresner, Some remarks on the integration of the extended Nernst–Planck equations in the hyperfiltration of multicomponent solutions, *Desalination*, 10 (1972) 27–46.
- [61] J. Lopez, A. Yaroshchuk, M. Reig, O. Gibert, J.L. Cortina, An engineering model for solute transport in semi-aromatic polymeric nanofiltration membranes: extension of solution–electro-diffusion model to complex mixtures, *J. Environ. Chem. Eng.*, 9 (2021) 105262, doi: 10.1016/j.jece.2021.105262.